A microslip friction model with normal load variation induced by normal motion

Ender Cigeroglu · Ning An · Chia-Hsiang Menq

Abstract A two-dimensional microslip friction model with normal load variation induced by normal motion is presented in this paper. The model is a distributed parameter model, which characterizes the stick-slip-separation of the contact interface and determines the resulting friction force, including its time variance and spatial distribution, between two elastic structures. When the relative motion is simple harmonic motion, the stick-slip-separation transition angles associated with any point in the contact area can be analytically determined within a cycle of motion. In addition, if the relative motion is given, stick-slip-separation transition boundaries inside the contact area and their time variances can be determined. Along with an iterative multi-mode solution approach utilizing harmonic balance method (HBM), the developed model can be employed to determine the forced response of frictionally constrained structures. In the approach, the forced response is constructed in terms of the free mode shapes of the structure; consequently, it can be determined at any excitation frequency and for any type of normal load distribution. Two examples, a one-dimensional beam like damper and a more realistic blade to ground damper, are employed to illustrate the predictive abilities of the developed model. It is shown that while

employing a single mode model, transition boundaries for the beam like damper agrees with the results given in the literature, the developed method identifies the phase difference along the slip to stick transition boundary when a multi-mode model is employed. Moreover, while partial slip is illustrated in the two examples, typical softening and hardening effects, due to separation of the contact surface, are also predicted for the blade to ground damper.

1 Introduction

Mechanical systems having frictionally constrained interfaces often involve complex contact kinematics induced by the relative motion between moving components [1, 2]. When the relative motion stays on the contact plane, the contact normal load remains constant during the course of motion and the interface experiences stick-slip friction induced by the tangential motion. This type of contact kinematics arises from either the specific design of friction contact [3, 4] or from the simplification of the analysis [5, 6]. More generally, if the relative motion has normal component perpendicular to the contact plane, the normal motion will cause normal load variation and possible intermittent separation of the two contacting surfaces. It can occur in

E. Cigeroglu · N. An · C.-H. Menq (✉)
Department of Mechanical Engineering, The Ohio State University, 231W, 18th Avenue, Columbus, OH, 43202, USA
e-mail: menq.1@osu.edu

various systems such as shroud contact interfaces of fan blades and wedge damper contact of turbine blades in turbine jet engines [7, 8].

In order to determine the forced response of shrouded fan stages, the stick-slip-separation analysis was undertaken by Menq et al. [9] in 1986, in which the normal motion was assumed to be in phase with the tangential motion and analytical formulas for the resulting contact friction force were derived. A more comprehensive model dealing with normal load variation was developed by Yang et al. [10] in 1998. They developed analytical criteria for stick-slip-separation transition when subjected to general time varying normal load and derived analytical formulas for transition angles when the relative motion was simple harmonic motion. The effect of normal load variation was also addressed by Yang and Menq [11] for three-dimensional harmonic motion in 1998 and by Chen et al. [12] for three-dimensional periodic motion in 2001. Later in 2003, utilizing the similar criteria developed in [10], Petrov and Ewins [13] published their work for one-dimensional tangential motion with normal load variation and described an algorithm to determine transition angles numerically for periodic motion, similar to that reported in [12]. They applied their method to a bladed disk system, in which each blade was connected to the neighboring blade through a single nonlinear element.

It should be noted that, all the above-mentioned friction models are for point contact, in which the entire interface is either in stick, slip, or separation states and partial slip is not possible. This so-called macroslip approach is widely used and works well if the normal load is small. However, microslip, or partial slip of the friction interface, becomes important and needs to be taken into account when the friction contact pressure is large. An interesting aspect of the microslip approach [14–18] is the assumption that the friction force is transmitted across a contact area rather than through a point of contact and that a distributed version of Coulomb's law of friction determines which part of the contact surface slips. The effects of microslip on the vibration of frictionally constrained structures and its significance were experimentally verified [15, 19, 20]. It is important to note that, due to its mathematical complexity, most of the models developed for microslip friction are for simple structures and for simple contact kinematics, which leaves real contact problems unaddressed.

Menq et al. [14] developed a continuous microslip friction model, in which an elastic bar having a uniform normal load distribution and in contact with the rigid ground was studied. A shear layer, which allows elastic deformations before the beginning of slip, was placed in between the rigid ground and the bar. The elastic bar is connected to a spring at the left end and analyzed under the effect of a static force applied at the right end. The developed microslip friction damper is analyzed with a single degree of freedom oscillator using Harmonic Balance Method, and the results indicated fifty percent reductions in the resonant response for high normal load distributions. Furthermore, this developed friction model was used to explain turbine blade friction damping data and shroud damping data in reference [15].

Based on the model developed in [14] and described above, Csaba [16] proposed a microslip friction model with a quadratic normal load distribution, where the shear layer is removed for simplicity. A single blade with a friction damper was analyzed and it was observed that predictions of vibration amplitudes from macroslip model were much higher than those of the microslip one. The beam model in [14] was also addressed by Quinn and Segalman [17]; where in order to investigate joint dynamics, authors obtained analytical expressions for quasi-static case excluding the inertial term, and developed a discrete model in order to numerically solve the same problem with the inertial effects included. From the numerical analysis, authors deduced that, for low frequency excitations, quasi-static model approximates the system response closely.

Cigeroglu et al. [18] developed a one-dimensional dynamic microslip friction model including the inertia of the damper, based on the beam model developed in [14]. Three different normal load distributions resulting in two distinct friction interfaces were considered and the analytical solutions considering the first vibration mode of the elastic bar were developed. The effect of excitation frequency on the hysteresis curves and Fourier coefficients was presented and the results obtained were compared with each other.

This paper presents a two-dimensional microslip friction model, in which the relative motion between the two contacting planes is two-dimensional and can be resolved into two components. The tangential component induces stick-slip friction while the normal component causes normal load variation and possible separation.

The model is a distributed parameter model, in which the transition criteria developed in [10] are employed to characterize the stick-slip-separation of the contact interface. Since only single harmonic motions are considered, the stick-slip-separation transition angles associated with any point in the contact area can be analytically determined within a cycle of motion. Consequently, the spatial distributions and time variances of these transition angles over the contact interface and the associated 2D contact friction maps can be determined. Along with an iterative multi-mode solution approach utilizing harmonic balance method (HBM), the obtained 2D contact friction maps can be employed to determine the forced response of frictionally constrained structures. In the approach, the forced response is constructed in terms of the free mode shapes of the structure. Consequently, it can be determined at any excitation frequency and for any type of normal load distribution. Two examples, a one-dimensional beam like damper and a more realistic blade to ground damper, are employed to illustrate the predictive abilities of the developed model.

2 Two-dimensional microslip friction model with normal load variation

In Fig. 1, planar contact of two bodies is given where the gray region is the contact interface composed of distributed springs, representing normal stiffness and tangential stiffness. The orientation of the contact plane is assumed to be invariant as the amplitude of vibration is relatively small. The global coordinate system is denoted by (x, y, z) with respect to which the displacements of bodies A and B are defined while (p, q, r) is the contact plane coordinate system where the contact plane is defined as $q = 0$. Any point in the contact plane coordinate system can be transferred to the global coordinate system by a translation and a rotation as follows:

$$\begin{bmatrix} x \\ y \\ z \end{bmatrix} = R \begin{bmatrix} p \\ q \\ r \end{bmatrix} + \begin{bmatrix} p_0 \\ q_0 \\ r_0 \end{bmatrix}. \quad (1)$$

In this equation, R is the orientation matrix and $[\, p_0 \; q_0 \; r_0 \,]^T$ is the position of (p, q, r) in (x, y, z). The spatial domain of the contact interface is specified in (p, q, r). Any point within the domain is denoted by
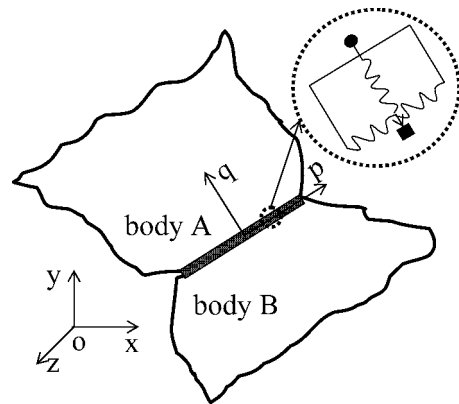

Fig. 1 Planar contact of two bodies

$[p_c \; 0 \; r_c]^T$ and its coordinate in (x, y, z) can be determined from the following equation

$$\begin{bmatrix} x_c \\ y_c \\ z_c \end{bmatrix} = R \begin{bmatrix} p_c \\ 0 \\ r_c \end{bmatrix} + \begin{bmatrix} p_0 \\ q_0 \\ r_0 \end{bmatrix}. \quad (2)$$

The contact preload and its distribution over the contact area can be determined through static analysis. When vibrating, the dynamic motions of the two bodies, associated with any contact point $[x_c \; y_c \; z_c]^T$ in (x, y, z), are denoted by $\mathbf{d}_A(x_c, y_c, z_c, t)$ and $\mathbf{d}_B(x_c, y_c, z_c, t)$, respectively, in which t is the temporal variable. The relative motion in (p, q, r) can then be determined from the following relation

$$\begin{bmatrix} u(p_c, r_c, t) \\ v(p_c, r_c, t) \\ w(p_c, r_c, t) \end{bmatrix} = R^{-1} [\mathbf{d}_A - \mathbf{d}_B]. \quad (3)$$

In general, the relative motion is three-dimensional and has tangential component $[u \; w]^T$ and normal component v. For simplicity, this paper focuses on a two-dimensional version, in which while the normal motion v is retained, the two bodies move with respect to each other on the contact plane back and forth along the p direction. In other words, the r component of the relative motion, w, is assumed to be zero, and the relative motion is characterized by the in-plane motion u and out of plane motion v, associated with p- and q-axis, respectively. The r-axis is used to define the contact interface together with the p-axis.

2.1 Stick, slip, and separation transition

A contact pair in the distributed contact model is illustrated in Fig. 2, in which $u(p, r, t)$, $v(p, r, t)$, $k_u(p, r)$, $s_u(p, r, t)$, $n_0(p, r)$ and $k_v(p, r)$ are the relative motion in the slip direction, relative motion in the normal direction, contact stiffness distribution in the slip direction, slip motion, preload distribution, and normal stiffness distribution, respectively. The two spatial variables, p and r, are specified on the contact plane and within the contact area, and their subscript "c" is removed for simplicity. The preload $n_0(p, r)$ is positive if the contact pair is preloaded. On the other hand, $n_0(p, r)$ is negative and in proportional to normal stiffness distribution $k_v(p, r)$ if it has an initial gap. The two-dimensional motion considered in the model is composed of two perpendicular components: tangential motion $u(p, r, t)$ in the p direction and the normal motion $v(p, r, t)$ in the q direction. The normal motion causes normal load variation and possible separation, according to the following equation,

$$n(p, r, t) = \begin{cases} n_0(p, r) + k_v(p, r)v(p, r, t), \\ \quad \text{if } v(p, r, t) \geq -n_0(p, r)/k_v(p, r) \\ 0, \\ \quad \text{if } v(p, r, t) < -n_0(p, r)/k_v(p, r) \end{cases} \tag{4}$$

and the resulting friction force is related to the tangential relative motion according to the following equation, if the slip motion $s_u(p, r, t)$ is known,

$$f(p, r, t) = k_u(p, r) [u(p, r, t) - s_u(p, r, t)]. \tag{5}$$

It is evident that in order to determine the slip motion and thus the resulting friction force, stick-slip-separation needs to be determined according to the tangential relative motion and normal motion. The stick-slip-separation transition criteria employed in this paper are based on those developed by Yang and Menq in [10].

2.1.1 Slip-to-stick transition

Transition from slip to stick state occurs when slip velocity, $\partial s_u / \partial t = 0$; and while slipping, friction force can be determined from
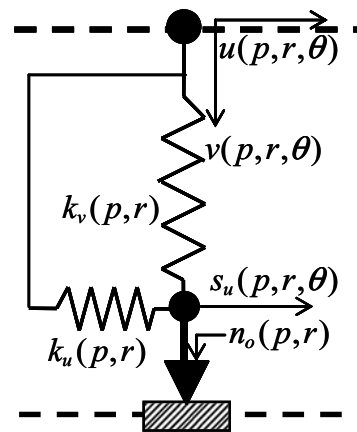
$$f(p, r, t) = \pm \mu n(p, r, t). \tag{6}$$

Fig. 2 Distributed contact model for 2D motion

Differentiating Equations (5) and (6) with respect to time and equating them, slip velocity is determined as follows:

$$\frac{\partial s_u}{\partial t} = \frac{\partial u}{\partial t} \pm \frac{\mu k_v(p, r)}{k_u(p, r)} \frac{\partial v}{\partial t}. \tag{7}$$

Using Equation (7), transition criteria from positive slip to stick and negative slip to stick are given as:

$$\frac{\partial u}{\partial t} - \frac{\mu k_v(p, r)}{k_u(p, r)} \frac{\partial v}{\partial t} = 0,$$

$$\frac{\partial^2 u}{\partial t^2} - \frac{\mu k_v(p, r)}{k_u(p, r)} \frac{\partial^2 v}{\partial t^2} < 0, \tag{8}$$

$$\frac{\partial u}{\partial t} + \frac{\mu k_v(p, r)}{k_u(p, r)} \frac{\partial v}{\partial t} = 0,$$

$$\frac{\partial^2 u}{\partial t^2} + \frac{\mu k_v(p, r)}{k_u(p, r)} \frac{\partial^2 v}{\partial t^2} > 0, \tag{9}$$

respectively. Inequalities in Equations (8) and (9) are used to guarantee slip to stick transition.

2.1.2 Stick-to-slip transition

Friction force at the stick state is given as follows

$$f(p, r, t) = k_u(p, r)[u(p, r, t) - u_0(p, r)]$$
$$\qquad + f_0(p, r), \tag{10}$$

where, $u_0(p, r)$ and $f_0(p, r)$ are distribution of displacement and friction force at the beginning of stick state. Stick to slip transition occurs when the friction force reaches to the slip load which can be determined by equating Equations (6) and (10). Transition from stick to positive-slip and from stick to negative-slip are:

$$k_u(p, r)[u(p, r, t) - u_0(p, r)] + f_0(p, r)$$
$$- \mu[n_0(p, r) + k_v(p, r)v(p, r, t)] = 0,$$
$$k_u(p, r)\frac{\partial u}{\partial t} - \mu k_v(p, r)\frac{\partial v}{\partial t} > 0, \qquad (11)$$
$$k_u(p, r)[u(p, r, t) - u_0(p, r)] + f_0(p, r)$$
$$+ \mu[n_0(p, r) + k_v(p, r)v(p, r, t)] = 0,$$
$$k_u(p, r)\frac{\partial u}{\partial t} + \mu k_v(p, r)\frac{\partial v}{\partial t} < 0, \qquad (12)$$

respectively. Again, inequalities given in Equations (11) and (12) are used to ensure the stick to slip transition.

2.1.3 Separation

Separation occurs when the friction interfaces loose contact and, beginning and end of separation can be determined from the following criteria:

$$n_0(p, r) + k_v(p, r)v(p, r, t) = 0, \quad \frac{\partial v}{\partial t} > 0, \qquad (13)$$

$$n_0(p, r) + k_v(p, r)v(p, r, t) = 0, \quad \frac{\partial v}{\partial t} < 0, \qquad (14)$$

respectively. At the end of separation the next state can be determined by the following criteria:

$$\text{Stick:} \quad -\frac{\mu k_v(p, r)}{k_u(p, r)}\frac{\partial v}{\partial t} < \frac{\partial u}{\partial t} < \frac{\mu k_v(p, r)}{k_u(p, r)}\frac{\partial v}{\partial t},$$
$$(15)$$

$$\text{Positive slip:} \quad \frac{\partial u}{\partial t} > \frac{\mu k_v(p, r)}{k_u(p, r)}\frac{\partial v}{\partial t}, \qquad (16)$$

$$\text{Negative slip:} \quad \frac{\partial u}{\partial t} < -\frac{\mu k_v(p, r)}{k_u(p, r)}\frac{\partial v}{\partial t}. \qquad (17)$$

It should be noted that, the friction coefficient in this analysis is taken as constant through out the contact interface; however, it can as well be considered as a distributed parameter and the same equations can be used if the distribution of friction coefficient is combined with the normal load distribution.

2.2 Transition angles

While the transition criteria given in Equations (8–17) can be applied to any arbitrary relative motion, the determination of transition angles often requires numerical simulation. Nonetheless, if the forced response is of interest and the relative motion is assumed to be single harmonic motion, stick-slip-separation transition angles can be determined analytically based on the derived criteria. Assuming the following form for the relative motions

$$u(p, r, \theta) = a(p, r)\sin(\theta),$$
$$v(p, r, \theta) = b(p, r)\sin(\theta + \varphi(p, r)), \qquad (18)$$

where $\theta = \omega t$ and, ω and t are the oscillation frequency and time, respectively; transition angles as a function of p and r are determined and expressed in terms of three dimensionless parameters, namely $\bar{b}(p, r) = \mu k_v(p, r)b(p, r)/k_u(p, r)a(p, r)$, $\varphi(p, r)$, and $\bar{n}_o(p, r) = \mu n_o(p, r)/k_u(p, r)a(p, r)$. Stick, slip, separation transitions in one cycle of motion can be categorized in three different groups: complete stick, stick-slip without separation and separation.

When the preload acting on the friction interface is high and the relative motion is small the friction interface sticks all the time and this can be identified by eliminating the criteria given in Equations (11) and (12), which can be characterized by the following inequality:

$$2\bar{n}_0(p, r) > \sqrt{1 + \bar{b}(p, r)^2 - 2\bar{b}(p, r)\cos[\varphi(p, r)]}$$
$$+ \sqrt{1 + \bar{b}(p, r)^2 + 2\bar{b}(p, r)\cos[\varphi(p, r)]}$$
$$(19)$$

Similarly, eliminating the criteria given in Equations (13) and (14), the condition for no separation can be derived as

$$\sqrt{1 + \bar{b}(p, r)^2 - 2\bar{b}(p, r)\cos[\varphi(p, r)]}$$
$$+ \sqrt{1 + \bar{b}(p, r)^2 + 2\bar{b}(p, r)\cos[\varphi(p, r)]} \qquad (20)$$
$$> 2\bar{n}_0(p, r) > \bar{b}(p, r).$$

2.2.1 Stick-slip but no separation

When the amplitude of the relative motion increases to some extent, the friction contact begins to slip but still remains in contact. In this case, the friction contact undergoes alternating stick-to-slip motion, which results in a hysteresis loop consisting of four alternating regions (positive-slip, stick, negative-slip and stick) separated by four transition angles. Substituting Equation (18) to Equations (8) and (9), positive-slip to stick and negative-slip to stick transition angles are derived as follows:

$$
\theta_P(p,r) = \pi - \psi(p,r) \\
- \arctan\left(\frac{1 - \bar{b}(p,r)\cos[\varphi(p,r)]}{\bar{b}(p,r)\sin[\varphi(p,r)]}\right),
$$
(21)

$$
\theta_N(p,r) = \pi - \psi(p,r) \\
+ \arctan\left(\frac{1 + \bar{b}(p,r)\cos[\varphi(p,r)]}{\bar{b}(p,r)\sin[\varphi(p,r)]}\right),
$$
(22)

where

$$
\psi(p,r) = \begin{cases} 0, & \text{if } 0 < \varphi(p,r) < \pi \\ \pi, & \text{if } \pi < \varphi(p,r) < 2\pi \end{cases}.
$$

Transition angles from stick to positive-slip and from stick to negative-slip are given as:

$$
\theta_{StP}(p,r) = \psi(p,r) + \arccos\left(\frac{\ell_2(p,r) - 2\bar{n}_0(p,r)}{\ell_1(p,r)}\right) \\
- \arctan\left(\frac{1 - \bar{b}(p,r)\cos[\varphi(p,r)]}{\bar{b}(p,r)\sin[\varphi(p,r)]}\right),
$$
(23)

$$
\theta_{StN}(p,r) = +\psi(p,r) + \arccos\left(\frac{\ell_1(p,r) - 2\bar{n}_0(p,r)}{\ell_2(p,r)}\right) \\
+ \arctan\left(\frac{1 + \bar{b}(p,r)\cos[\varphi(p,r)]}{\bar{b}(p,r)\sin[\varphi(p,r)]}\right),
$$
(24)

where

$$
\ell_1(p,r) = \sqrt{1 + \bar{b}(p,r)^2 - 2\bar{b}(p,r)\cos[\varphi(p,r)]},
$$
$$
\ell_2(p,r) = \sqrt{1 + \bar{b}(p,r)^2 + 2\bar{b}(p,r)\cos[\varphi(p,r)]}.
$$

2.2.2 Separation

If separation exists, hysteresis loop is composed of 10 possible sequences of alternating stick-slip-separation which are characterized by six transition angles. From the criteria given in Equations (13) and (14), start and end of separation angles are derived as

$$
\theta_{Sp1}(p,r) = \pi + \arcsin\left(\frac{\bar{n}_0(p,r)}{\bar{b}(p,r)}\right) - \varphi(p,r), \quad (25)
$$

$$
\theta_{Sp2}(p,r) = -\arcsin\left(\frac{\bar{n}_0(p,r)}{\bar{b}(p,r)}\right) - \varphi(p,r). \quad (26)
$$

Transition angels for positive-slip to stick and negative-slip to stick are given in Equations (21) and (22), respectively. The transition angels from negative-slip-stick to positive-slip and positive-slip-stick to negative-slip can be obtained from Equations (23) and (24); however, if the previous state of stick is separation then transition angles from separation-stick to positive-slip and separation-stick to negative-slip are given as

$$
\theta_{SpP}(p,r) = \pi - \psi(p,r) \\
- \arccos\left(\frac{\sin[\theta_{Sp2}(p,r)] + \bar{n}_0(p,r)}{l_1(p,r)}\right) \\
- \arctan\left(\frac{1 - \bar{b}(p,r)\cos[\varphi(p,r)]}{\bar{b}(p,r)\sin[\varphi(p,r)]}\right),
$$
(27)

$$
\theta_{SpN}(p,r) = \psi(p,r) \\
+ \arccos\left(\frac{\sin[\theta_{Sp2}(p,r)] - \bar{n}_0(p,r)}{l_2(p,r)}\right) \\
+ \arctan\left(\frac{1 + \bar{b}(p,r)\cos[\varphi(p,r)]}{\bar{b}(p,r)\sin[\varphi(p,r)]}\right).
$$
(28)

Since the analytical distribution of transition angles are known, it is possible to determine stick-slip-separation (friction interface) map at any instant. This friction interface map is useful to understand how the friction damper works and it can as well be used to estimate wear of the contacting surfaces.

2.3 Stick-slip-separation map

It has been shown that if the relative motion is given and assumed to be single harmonic motion, analytical expressions for transition angles in terms of the two spatial variables are available. These expressions, $\theta(p, r)$, can be visualized as three-dimensional surfaces. The stick-slip-separation map at any instant is composed of stick-slip-separation transition boundaries, which can be determined by intersecting those 3D surfaces with the associated constant θ value. Moreover, the time variance of this friction interface map can be illustrated by changing θ value. In this work, stick-slip-separation map is used to demonstrate the microslip phenomenon, whereas it can as well be employed to estimate component wear caused by the rubbing of contact surfaces. Some of the factors affecting wear of sliding surfaces are duration of sliding, normal load, and friction (tangential) force acting on the contact interface. Normal load and friction force distributions are already determined from the developed friction model and the duration of sliding can be obtained from the stick-slip-separation map, which can be used to estimate the wear of sliding surfaces.

2.4 Distribution of Fourier coefficients

Given the relative motion, which is assumed to be single harmonic motion, transition angles, and thus the resulting friction force over a cycle of motion, are known analytically. If the forced response is of interest, the resulting friction force can be approximated by its Fourier components.

$$f(p, r, \theta) \cong f_b(p, r) + f_s(p, r) \sin(\theta)$$
$$+ f_c(p, r) \cos(\theta), \quad (29)$$

where $f_b(p, r)$ is the distribution of the mean force, $f_s(p, r)$ spring force, and $f_c(p, r)$ damping force. For the same purpose, the Fourier coefficients of the variable normal load can be derived. These distribution functions illustrate the spatially distributed dynamic characteristics of the contact friction interface.

3 Forced response

Finite element models are often used in the forced response analysis of complex structures, which result in many degrees of freedom (DOF). Due to the friction contact, this results in large systems of nonlinear equations which need to be solved iteratively. This is a computationally expensive and also an inefficient process. Menq and Griffin [21] in 1985 developed a nonlinear forced response analysis method for steady state response of frictionally damped structures using finite element models. In the developed method, using the receptance of the linear system, authors considered only the nonlinear DOF first and determined the harmonic displacement of these DOF by an iterative solution procedure. Using these displacements, the forces acting on these DOF were obtained, and treating them as external forces and together with the excitation forces, authors determined the response of the complete structure. This method reduces the number of nonlinear equations to the number of nonlinear DOF, and it is a very efficient method to analyze frictionally constrained structures, since the nonlinearity comes only from the frictionally constraint DOF. Structural modification techniques were as well applied by Tanrıkulu et al. [22], Sanliturk et al. [23] and Ciğeroğlu and Özgüven [24] in order to solve large nonlinear equation systems, where the dynamic stiffness matrix of the nonlinear system was determined by applying structural modifications to dynamic stiffness matrix of the linear system.

The methods explained above can as well be applied to model microslip friction; however, many friction elements are needed in microslip modeling which results in large number of nonlinear DOF. Moreover, if the bladed disk system is mistuned, since the cyclic symmetry of the structure is destroyed; all the blade-damper sectors have to be included into the forced response analysis resulting in even larger nonlinear equation systems. It should be noted that, the finite element models for bladed disk systems contain many DOF; thus, even for linear forced response analysis, reduction techniques are employed [25–27]. In this work, a modal superposition technique is used, where the motion of the frictionally constrained structure is assembled from its free mode shapes. In this approach, the number of unknowns depends on the number of mode shapes used in the modal expansion process, which decreases the number of nonlinear equations significantly even for microslip models.

3.1 Multi-mode solution method

Equation of motion in matrix form for a system with dry friction dampers can be written in the following form

$$\mathbf{M}\ddot{X} + \mathbf{C}\dot{X} + \mathbf{K}X = F_e(t) + F_n(X),\qquad(30)$$

in global coordinate system, where $\mathbf{M}$, $\mathbf{C}$, $\mathbf{K}$, $F_e(t)$, $F_n(X)$, and X are the mass matrix, viscous damping matrix, stiffness matrix, excitation force vector, nonlinear friction force vector and relative displacement vector, respectively. The 2D microslip friction model developed is defined on the contact plane coordinate system. Therefore, the nonlinear friction and normal forces obtained from the model are as well in the contact plane coordinate system. Displacement vector X in global coordinates can be written as

$$X(B, A, x, y, z) = \sum_{n=1}^{N} B_n \phi_n(x, y, z)$$
$$+ \mathrm{Re}\left(\sum_{n=1}^{N} A_n \phi_n(x, y, z)e^{i\theta}\right),\qquad(31)$$

where ϕ_n, B_n, A_n, and N are the nth mode shape of frictionally constrained structure in global coordinate system, n^{th} real and complex modal coefficients for dc and ac components of motion, and number of modes used in the modal expansion process, respectively. Transforming X to contact plane coordinates, the relative motion of friction interface points in contact plane coordinates can be expressed as a function of the modal coefficient vectors

$$u = u(B, A, p, r, \theta),\qquad(32)$$
$$v = v(B, A, p, r, \theta),\qquad(33)$$

where B and A are the real and complex modal coefficient vectors for dc and ac components of motion, respectively. The nonlinear (friction and normal) force vector in contact plane coordinate system can be written similar to Equation (29) using the relative displacements given by Equations (32) and (33) as

$$^cF_n(B, A, p, r, \theta) \cong F_b(B, A, p, r)$$

$$+ F_s(B, A, p, r)\sin\theta + F_c(B, A, p, r)\cos\theta.\qquad(34)$$

Using the orthogonality of mode shapes, Equation (30) can be simplified to

$$(\mathbf{\Omega} - \omega^2\mathbf{I} + i\omega\mathbf{C}_r)A = Q_s^e + iQ_c^e + Q_s(B, A)$$
$$+ iQ_c(B, A),\qquad(35)$$
$$\mathbf{\Omega}B = Q_b(B, A),\qquad(36)$$

if mass normalized mode shapes are used. Here Q_s^e and Q_c^e are the in phase and out of phase modal force vectors for the excitation forces, Q_b, Q_s and Q_c are the modal force vectors for mean, spring and damping forces, $\mathbf{\Omega}$ is $N \times N$ diagonal matrix of squares of natural frequencies and $\mathbf{C}_r$ is the modal damping matrix, which is diagonal if the damping is proportional. The modal forcing vectors on the right hand side of Equations (35) and (36) are

$$Q_s^e = \iiint_{D_e} \left[\phi_{u_n}(p, q, r)f_{s_u}^e(p, q, r)\right.$$
$$\left. + \phi_{v_n}(p, q, r)f_{s_v}^e(p, q, r)\right]dp\,dq\,dr$$
$$Q_c^e = \iiint_{D_e} \left[\phi_{u_n}(p, q, r)f_{c_u}^e(p, q, r)\right.$$
$$\left. + \phi_{v_n}(p, q, r)f_{c_v}^e(p, q, r)\right]dp\,dq\,dr,\qquad(37)$$

$$Q_{*_n}(B, A) = \iint_D \left[\phi_{u_n}(p, 0, r)f_{*_u}(B, A, p, r)\right.$$
$$\left. + \phi_{v_n}(p, 0, r)f_{*_v}(B, A, p, r)\right]dp\,dr,\qquad(38)$$

where ϕ_{u_n} and ϕ_{v_n} are the nth mode shapes of the frictionally constrained structure in contact plane coordinates; f^e and f represent the excitation and nonlinear contact forces in contact plane coordinates; $*$ corresponds to s, c, or b; and u and v indicate the direction of mode shapes and forces along p and q axes, respectively. In addition to this D_e and D are the domain of integrations for the excitation and contact forces, respectively. Since the modal force vectors are in modal coordinates, they can be obtained using the

mode shapes and forcing vectors in contact plane coordinate system as given in Equations (37) and (38). This reduces the order of integration in Equation (38) from triple to double integration, since the contact interface D is a 2D plane area in contact plane coordinate system whereas it is a 3D surface in global coordinate system. Equations (35) and (36) describe a set of nonlinear algebraic equations and the unknown modal coefficient vectors B and A can be solved by an iterative nonlinear solver. It should be noted that, the total number of unknowns in this nonlinear equation set is $3N$, which is equal to the number of terms used in the Fourier series expansion multiplied by the number of mode shapes used in the modal expansion; and once the modal coefficient vectors are obtained, the motion of the frictionally constrained structure can be constructed.

4 Examples

Two examples, a one-dimensional bar-like damper and a more realistic blade to ground damper, are employed to illustrate the predictive abilities of the developed model.

4.1 1D bar model

This example is of interest because related results are given in the literature. The analytical solution procedure developed in [18] uses single mode information of a bar like damper to derive analytically the spatial boundary of the stick-slip transition for specific normal load distribution. Owing to the complicity of the stick-slip transition, solutions are limited to the range of first vibration mode and for three different normal load distributions, which are time invariant. On the other hand,

the method presented in this paper is capable of dealing with multi-mode vibration and with normal load that has arbitrary spatial distribution and is time variant. However, for the purpose of comparison, the normal load will be kept time invariant in this example, and the focus will be on the effect of number of modes used in the analysis.

A 1D bar model similar to the one in [18] is given in Fig. 3, where E, A, ρ, L, β, $q(x)$ and $F(t)$ are the modulus of elasticity, cross-sectional area, density, and length of the bar, strain hardening stiffness, normal load distribution and excitation force, respectively. The shear layer in [18] is replaced by distribution of contact stiffnesses in slip direction, $k_u(x)$. For harmonic forcing, partial differential equation for this system is

$$EA \frac{\partial^2 u}{\partial x^2} - \rho A \omega^2 \frac{\partial^2 u}{\partial \theta^2} = \tau(u, x) - F_0 \delta(x - L) \sin(\theta),$$
(39)

$$EA \left. \frac{\partial u}{\partial x} \right|_{x=0} = \beta u(0, \theta), \quad EA \left. \frac{\partial u}{\partial x} \right|_{x=L} = 0,$$
(40)

where u is the displacement of point x, $\tau(u, x)$ is the friction force distribution acting on the bar; F_0 is the amplitude of the harmonic forcing; δ is the Dirac delta function. The motion of the bar for harmonic excitation can be represented by its free mode shapes, which are analytically available for this case, using Equation (31). This is a one-dimensional bar problem hence, there is no z dependence; in addition to this, since the normal load is time invariant dc component of the motion and the friction force vanishes. Inserting Equation (32) into Equation (39) and applying the integral orthogonality
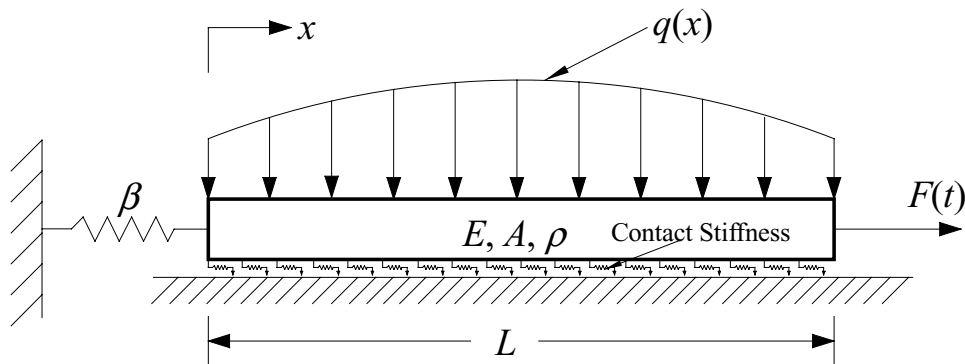

Fig. 3 1D bar model

relations, Equation (35) is obtained which can be solved for the unknown complex modal coefficients. An iterative solution procedure is applied to solve the nonlinear algebraic equations given in Equation (35) and the motion of the bar is constructed using the determined modal coefficients. The friction interfaces for the bar are determined for different normal load distributions, and the effect of number of modes used in the calculations is as well presented.

4.1.1 Friction interface

The model given in Fig. 3 is analyzed for constant and concave quadratic normal load distributions, which are defined in [18]. It should be noted that the analytical results given in [18] are derived for displacement input and the method presented in this paper is a forced response method. Therefore, their results can not be compared directly. Figures 4 and 5 show the build-up of friction force for constant and quadratic normal load distributions at 1000 Hz, which is around the first mode of the system. In the figures, 1 and −1 denote positive

and negative slip, respectively, and in between them lies the stuck region. Solid lines on the figures are the stick-slip boundary, which can be obtained from the transition angle equations derived in Section 2. It is seen that for constant normal load distribution, slip starts from the right end of the bar and propagates toward the left end, which will cause gross-slip if the excitation force is increased further. For quadratic normal load distribution, slip starts somewhere around the center of the bar and propagates toward both the ends. It first reaches the right end of the beam and then the left end resulting in gross-slip. These results are in agreement with the results obtained in [18], where the authors divide the contact interface into slip and stick regions and provide the change of length of each region for displacement input and similar normal load distributions.
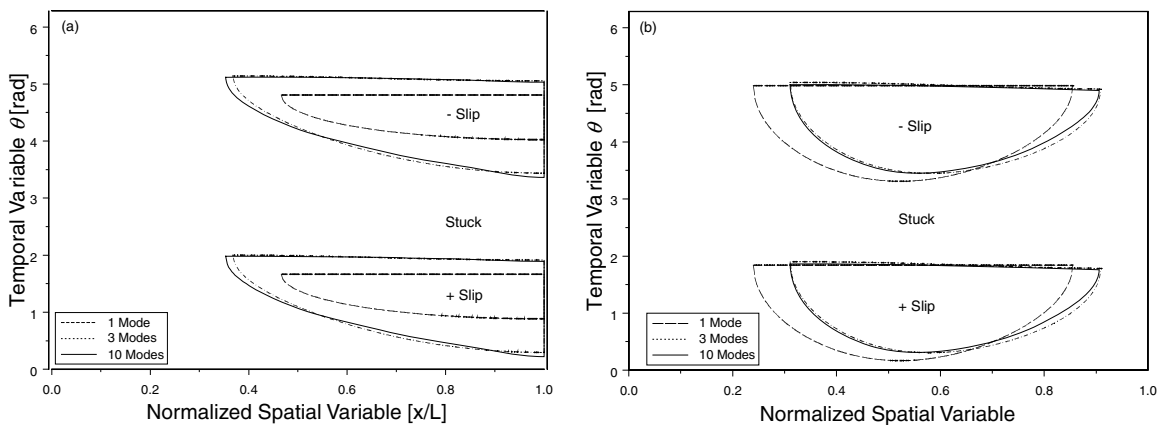
4.1.2 Effect of multiple modes

In order to demonstrate the effect of number of modes used in the analysis, constant and quadratic normal distribution cases are analyzed using single mode, 3
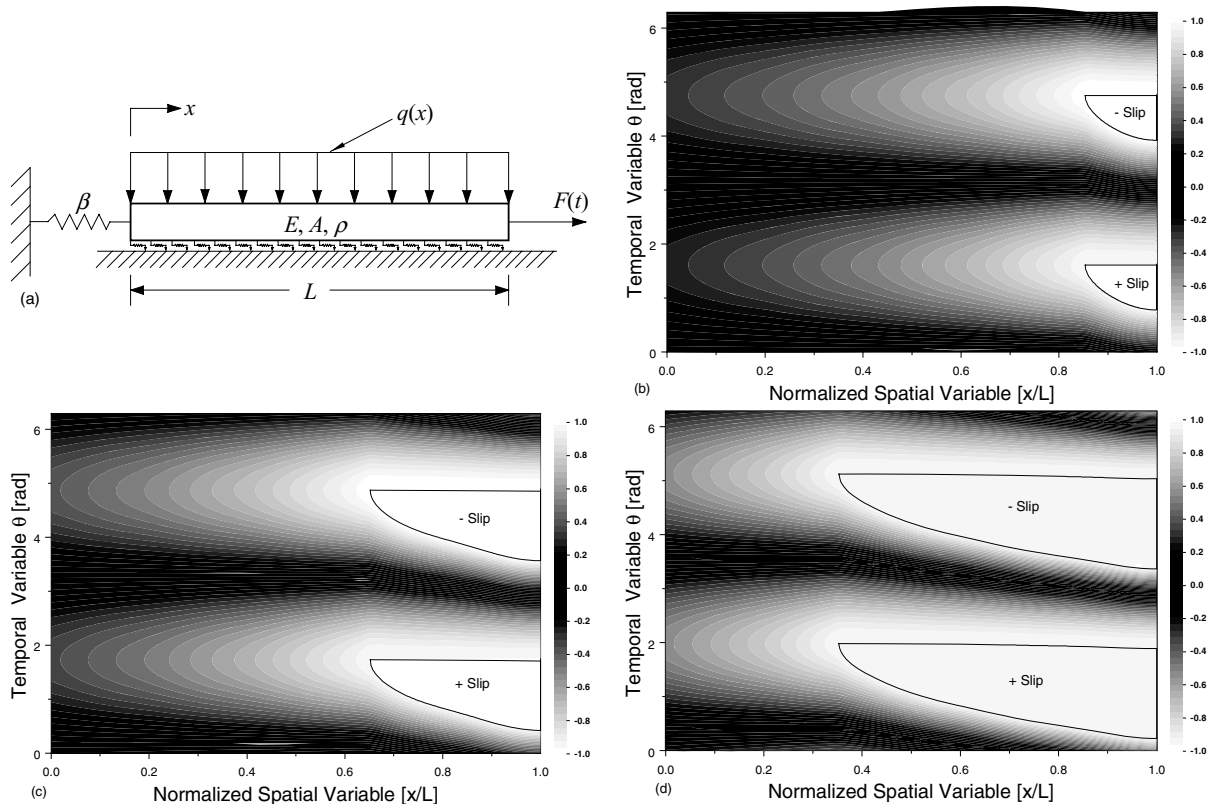
**Fig. 4** Build-up friction force for constant normal load distribution: (a) model, $F(t)$ for (b < c < d)
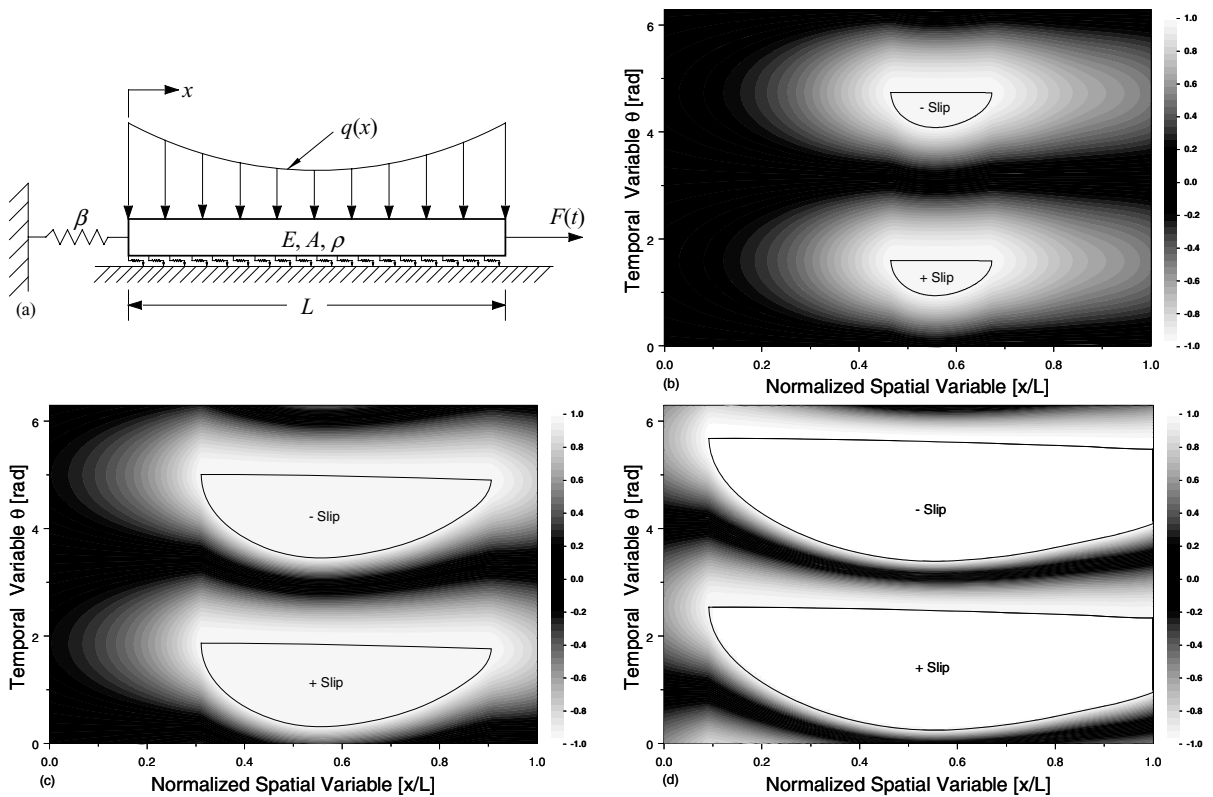
Fig. 5 Build-up friction force for quadratic normal load distribution: (a) model, $F(t)$ for (b < c < d)


Fig. 6 Effect of number of modes at 1000 Hz (a) constant (b) quadratic normal load distributions: 1 mode (- - - - - -), 3 modes (· · · · · ·), 10 modes (——)

modes and 10 modes of the system. The analyses are performed at 1000 Hz and 3100 Hz, which are around the first and second modes of the system and the stick-slip boundaries are given in Figs. 6 and 7. It is seen that, for all the cases 3-mode solution and the 10-mode solution result in similar friction interfaces. However, it is also seen that, even though single mode solution can

estimate the overall behavior of the friction interface, the results obtained may not be accurate. It should as well be noted that, single mode solution predicts the transition from slip to stick occurs at the same time for all the slipping points; however, that transition from slip to stick in multi-mode solution does not occur at the same instant. This is an expected result due to the
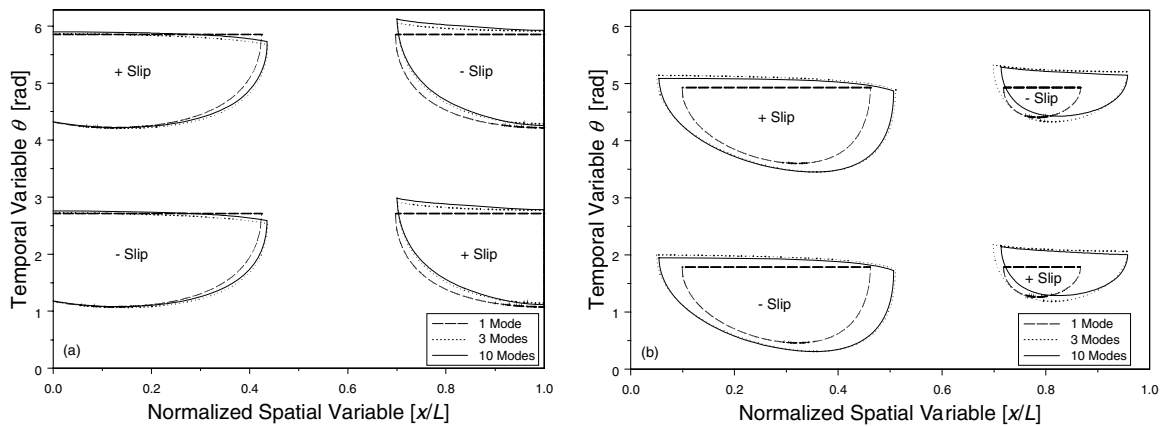
Fig. 7 Effect of number of modes at 3100 Hz (a) constant (b) quadratic normal load distributions: 1 mode (- - - - -), 3 modes (· · · · ·), 10 modes (——)
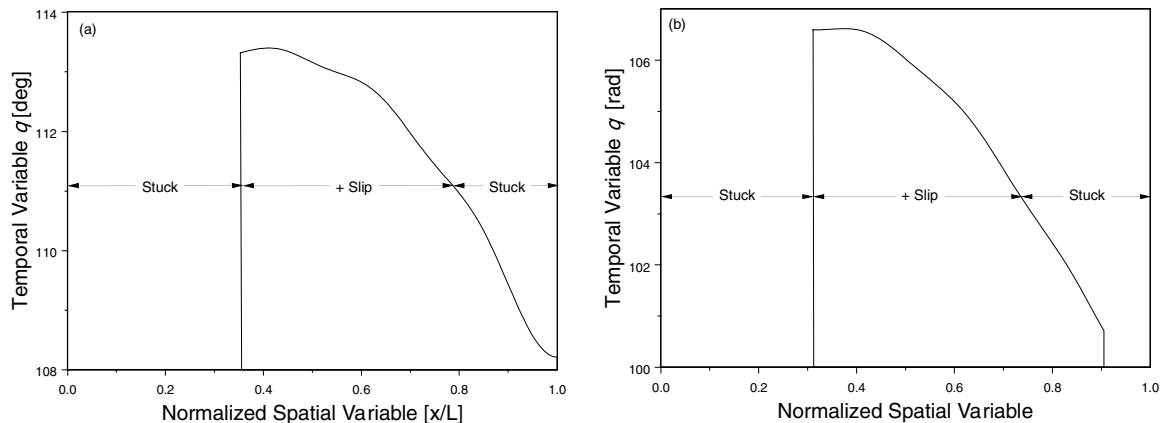
Fig. 8 Phase difference along slip to stick transition boundary at 1000 Hz (a) constant (b) quadratic normal load distributions

inertia of the bar and it becomes more evident in Fig. 7. Figure 8 shows the slip to stick transition that is predicted by the ten-mode solution and is zoomed into a very small range of θ.

4.2 Blade to ground damper

The blade to ground damper system analyzed is given in Fig. 9, where the right side of the platform of the blade is in contact with the ground. In this system, the blade is represented by a finite element model as shown in Fig. 10, in which B and B′ are two symmetric points, where excitation forces are applied and A is the point, where the displacements are calculated. Modal information and the mode shapes of the blade are obtained by a finite element analysis and inserted in Equations (35) and (36). It is assumed that the system is proportion-

ally damped with a damping ratio of 0.2%. Continuous mode shape functions are determined by applying curve fitting to the ones obtained by the finite element analysis. Unknown forcing vectors in Equations (35) and (36) are determined by Equation (38) using the continuous mode shape functions obtained by curve fitting. An iterative nonlinear solver is used to determine the unknown modal coefficients, from which the motion of the blade can be constructed by using Equation (31). In the following sections forced response results and stick-slip-separation maps for the blade to ground damper are presented.

4.2.1 Forced response results

Forced response curves for the blade to ground damper system are shown in Figs. 11 and 12, corresponding two

Fig. 9 Blade to ground damper model
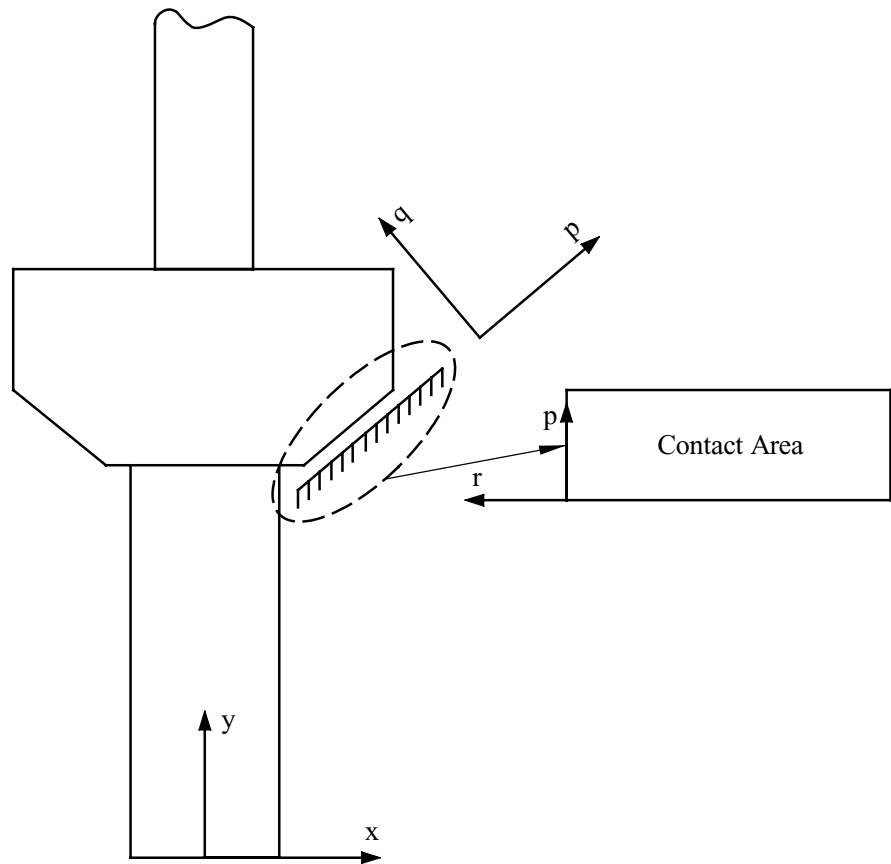
distinct forcing directions: x and y directions, respectively. Each forced response curve is associated with a specific preload or initial gap, and is around the first resonance of the system. For simplicity, uniform preload distribution over the contact surface is assumed and the total preload is specified in the two figures. It should be noted that, the effects of higher modes ($n > N$) on the displacements can be represented by residual stiffnesses which can be determined through finite element analysis and this information is used in the determination of tangential and normal contact stiffnesses; in addition, these contact stiffnesses make it possible to use lower frequency (higher wavelength) modes to determine microslip on the contact surface. In the analyses of the blade to ground damper, 10 modes of the blade are used. Forced response for free and stuck cases, which are the two linear extreme cases for the system, are as well included in the figures. The nonlinear response of the system is in between these two linear solutions and as the preload increases the peak frequency shifts to the right and the system response approaches to the stuck

response, finally becoming completely stuck. It is seen that, there exists an optimum value for the preload, which results in minimum displacement amplitude for each of the two cases. It should be noted that the vibration amplitude in Fig. 11 is about 20 times greater than that in Fig. 12. This is due to the fact that the first vibration mode of the blade, which is a bending mode around the z-axis, is less sensitive to the forcing in the y direction. It is as well interesting to note that, for this case the stuck response has higher displacement amplitude compared to that of the free response.

For high preloads, blade and ground are always in contact, i.e. there is no separation in the friction interface. However, as the preload acting on the friction interface decreases, normal motion of the blade results in separation in the contact interface, which shows itself as a softening effect in the forced response results. On the contrary, if the initial gap between the blade and the ground is decreased, due to the motion in normal direction, blade and ground come into contact resulting in hardening effect. It is possible to observe
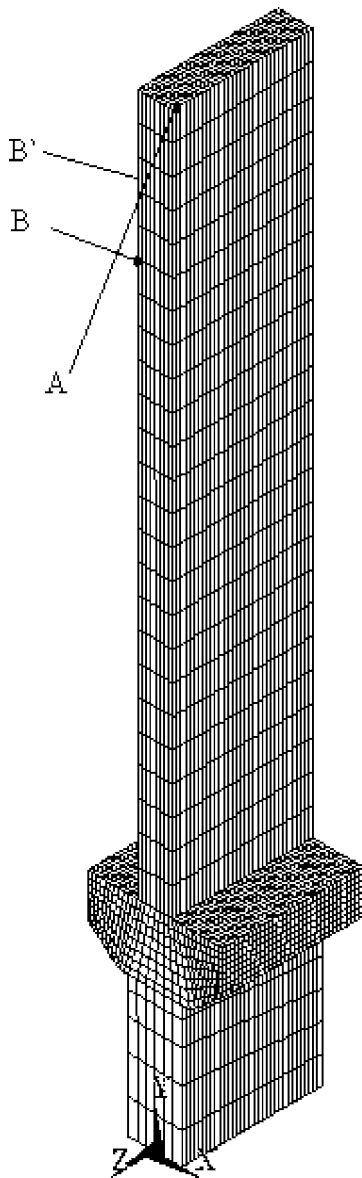
Fig. 10 Finite element model for the blade

jump phenomena in case of softening and hardening; therefore, continuation method is used to determine the forced response curves for those cases where there exists an unstable solution branch between two jumps. It should be noted that, unstable solution can not be obtained by time domain simulation, since the system response will converge to one of the two stable solutions unless the initial guess is exactly the unstable solution. Figure 13 shows the forced response curve for $n'_0 = 1000$. In Fig. 11, the unstable solution is iden-

tified by the dashed line. It should be noted that, the actual preload distribution acting on the contact interface depends on the dc component of the motion and the contact stiffness in the normal directions as

$$n_0(p, r) = n'_0(p, r) - k_v(p, r) v_0(p, r), \qquad (41)$$

where $n'_0(p, r)$ is the applied initial preload distribution on the contact interface and $v_0(p, r)$ is the distribution of dc component of the motion in the normal direction.
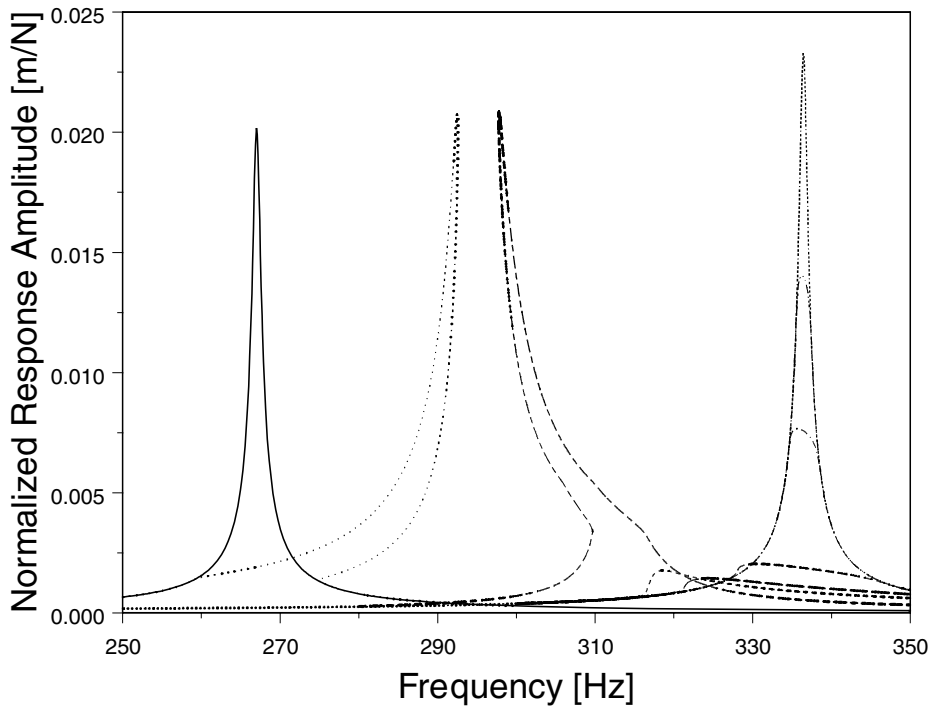
4.2.2 Friction interface

In order to illustrate the microslip phenomenon, the stick-slip-separation boundaries for the case of $n'_0 = 1000$, Fig. 13, is examined. Fiction interface maps associated with the excitation frequency at 296.038 Hz are obtained. Specifically, the maps before and after jump are plotted in Fig. 14, in which the left column is before the jump and the right column after the jump. It is evident that before the jump the vibration amplitude is significantly greater and the friction interface is not in contact most of the time; whereas, after the jump positive and negative slip states govern most of the friction interface. Therefore, it can be concluded that, jump in the forced response curve is due to the separation of the contact interface caused by the normal load variation. Fig. 15 shows the transition map when $\theta = 125°$. It is obvious that at this instant the contact interface is governed by three distinct states. In other word, over the contact interface one area is stuck, another area is slipping while the other has separation. This clearly demonstrates the microslip phenomenon.
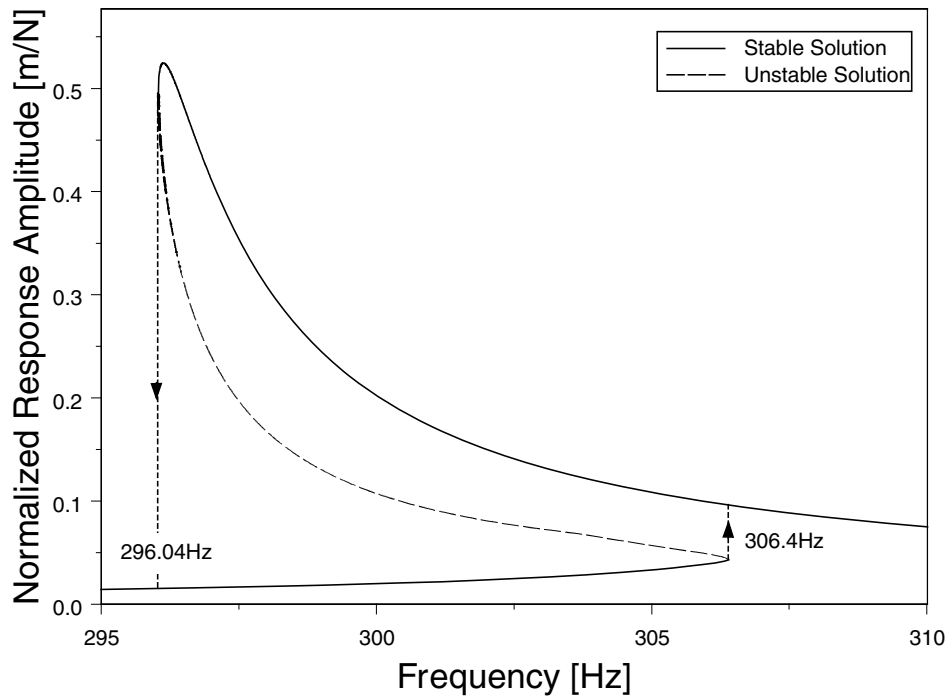
5 Conclusion

A distributed parameter model is developed to characterize the stick-slip-separation of the contact interface and determines the resulting friction force, including its time variance and spatial distribution, between two elastic structures. A multi-mode solution approach is developed to determine the forced response and stick-slip-separation transitions of the steady state solution of frictionally constrained structures when subjected to harmonic excitation. In the proposed approach, steady state response of the system is constructed by its free mode shapes. The proposed method is applied to a
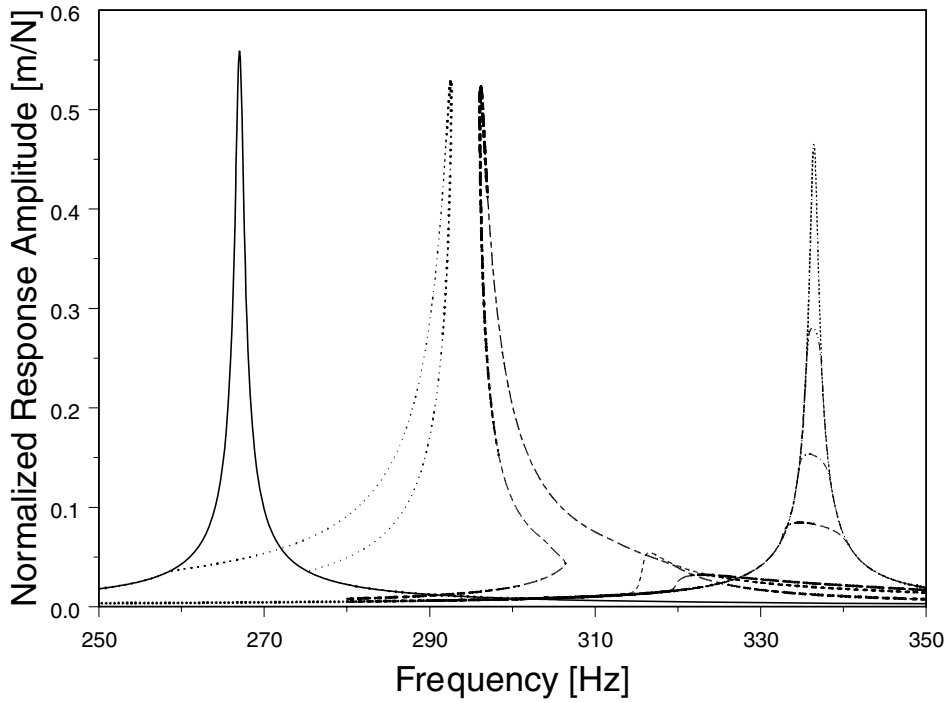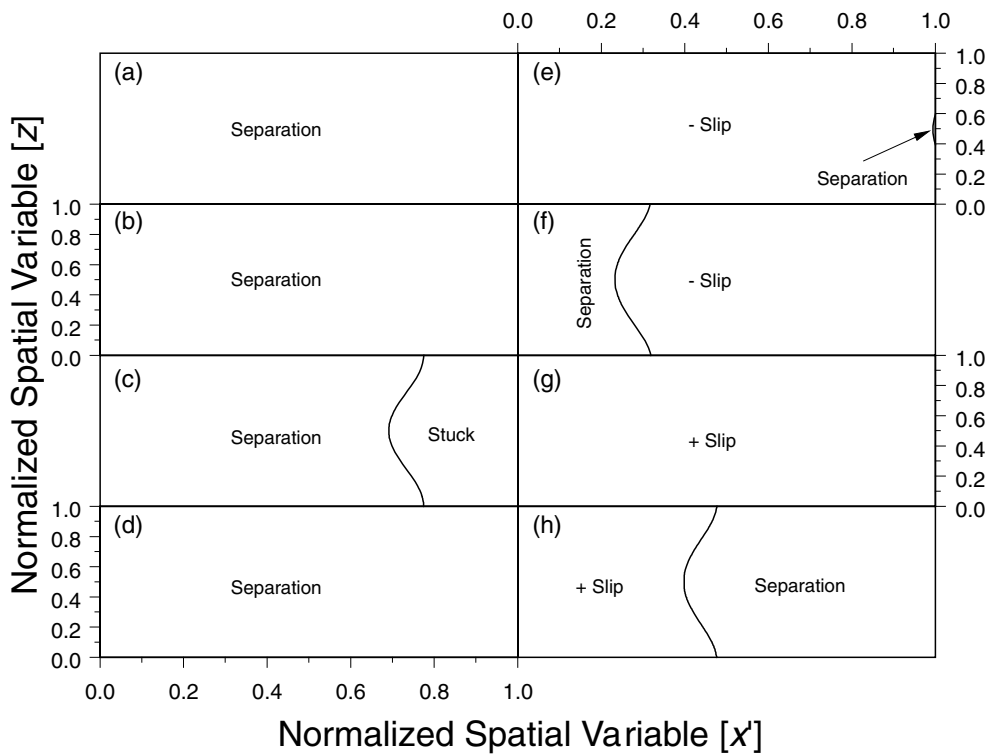
Fig. 11 Forced response for excitation force in x direction: free (——), $-5e5$ ($\cdots\cdots$), 1000 (–––––), 7500 (- - - - - -), 1e4 (– – –), 5e4 (- - - - -), 1e5 ($\cdot\text{-}\cdot\text{-}\cdot\text{-}\cdot$), 2e5 ($\cdot$ ------------), stuck ($\cdot\cdot\ \cdot\cdot\ \cdot\cdot$)

Fig. 12 Forced response for excitation force in y direction: free (——), $-2e4$ ($\cdots\cdots$), 80 (–––––), 350 (- - - - - -), 500 (– – –), 1000 (- - - - - -), 1e4 (- - - - - -), 2e4 ($\cdot\ \text{–}\ \cdot\ \text{–}\ \cdot$), stuck ($\cdot\cdot\ \cdot\cdot\ \cdot\cdot$)
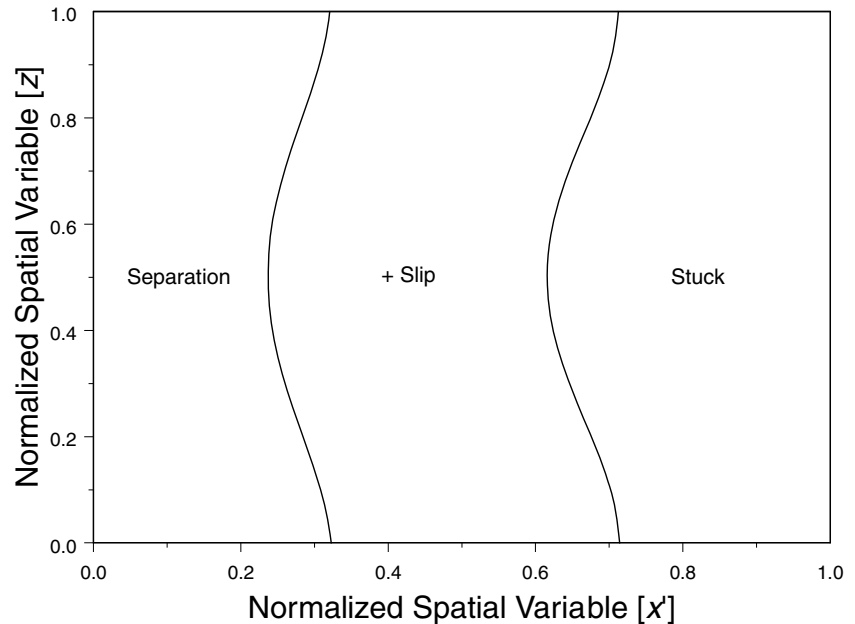
Fig. 13 Stable and unstable solutions for $n'_0 = 1000$: (——) stable solution, (– – –) unstable solution

Fig. 14 Friction interface for $n'_0 = 1000$ before jump: (a) 0°, (b) 90°, (c) 180°, (d) 270°. After jump: (e) 0°, (f) 90°, (g) 180°, (h) 270°

Fig. 15 Friction interface for $n_0' = 1000$ and $\theta = 125°$

one-dimension bar like damper. It is shown that while employing a single mode model, transition boundaries for the bar like damper agree with the results given in the literature, the developed method identifies the phase difference along the slip to stick transition boundary when a multi-mode model is employed.

The proposed method is also applied to a more realistic blade to ground damper model, where the blade is modeled by the finite element method. For this system, due to the complicated geometry analytical mode shapes are not available; hence, continuous functions are fitted to the finite element mode shapes and used in the analysis. Resulting forced response curves and transition maps are obtained and they clearly show the microslip phenomenon. Typical softening and hardening effects, due to separation of the contact surface, are also predicted for the blade to ground damper.

Although the relative motion between two contacting bodies is in general three-dimensional, for simplicity, this paper focuses on a two-dimensional version, in which while the normal motion v is retained, the two bodies move with respect to each other on the contact plane back and forth along the p direction. Nevertheless, it is possible to extend the method to general three-dimensional problem so that it can be applied to many real-world systems. It should as well be noted that, in order to apply the proposed method, in-plane and out of plane contact stiffness distributions in the

contact interface have to be determined. This issue will be discussed in future investigation.

References

1. Padmanabhan, C.: Analysis of periodically excited systems with clearances. Ph.D. thesis, The Ohio State University (1994)
2. Yang, B.D.: Contact kinematics of friction interfaces and applications to the prediction of resonant response of frictionally constrained turbine blades Ph.D. thesis, The Ohio State University (1996)
3. Griffin, J.H.: Friction damping of resonant stresses in gas turbine engine airfoils. J. Eng. Power-Trans. ASME **102**, 329–333 (1980)
4. Dowell, E.H., Schwartz, H.B.: Forced response of a cantilever beam with a dry friction damper attached, part I: Theory. J. Sound Vib. **91**, 255–267 (1983)
5. Cameron, T.M., Griffin, J.H., Kielb, R.E, Hoosac, T.M.: An integrated approach for friction damper design. ASME J. Vib. Acous. Stress Reliab. Design Trans. **112**, 175–182 (1990)

6. Ferri, A.A.: Friction damping and isolation systems. ASME J. Vib. Acoust. Trans. **117(B)**, 196–206 (1996)

7. Menq, C.H., Griffin, J.H., Bielak, J.: The forced response of shrouded fan stages. ASME J. Vib. Acous. Stress Reliab. Design Trans. **108**, 50–55 (1986)

8. Yang B.D., Menq C.H.: Characterization of contact kinematics and application to the design of wedge dampers in turbomachinery blading: part I: stick-slip contact kinematics. ASME J. Eng. Gas Turbines Power Trans. **120**(2), 410–417 (1998)

9. Menq, C.H., Griffin, J.H., Bielak, J.: The influence of a variable normal load on the forced vibration of a frictionally damped structure. J. Eng. Gas Turbines Power **108**, 300–305 (1986)

10. Yang, B.D., Chu, M.L., Menq, C.H.: Stick-slip-separation analysis and non-linear stiffness and damping characterization of friction contacts having variable normal load. J. Sound Vib. **210**, 461–481 (1998)

11. Yang, B.D., Menq, C.H.: Characterization of 3D contact kinematics and prediction of resonant response of structures having 3D frictional constraint. J. Sound Vib. **217**, 909–925 (1998)

12. Chen, J.J., Menq, C.H.: Periodic response of blades having three-dimensional nonlinear shroud constraints. J. Eng. Gas Turbines Power **123**, 901–909 (2001)

13. Petrov, E.P., Ewins, D.J.: Analytical formulation of friction interface elements for analysis of nonlinear multi-harmonic vibrations of bladed disks. J. Turbomach. **125**, 364–371 (2003)

14. Menq, C.H., Bielak, J., Griffin, J.H.: The influence of microslip on vibratory response, Part I A new microslip model. J. Sound Vib. **107**, 279–293 (1986)

15. Menq, C.H., Bielak, J., Griffin, J.H.: The influence of microslip on vibratory response, Part II A comparison with experimental results. J. Sound Vib. **107**, 295–307 (1986)

16. Csaba, G.: Forced response analysis in time and frequency domains of a tuned bladed disk with friction dampers. J. Sound Vib. **214**, 395–412 (1998)

17. Quinn, D.D., Segalman, D.J.: Using series-series Iwan-type models for understanding joint dynamics. J. Appl. Mech. **72**, 666–673 (2005)

18. Cigeroglu, E., Lu, W., Menq, C.H.: One-dimensional dynamic microslip friction model. J. Sound Vib. **292**, 881–898 (2006)

19. Filippi, S., Akay, A., Gola, M.M.: Measurement of tangential contact hysteresis during microslip. J. Tribol. **126**, 482–489 (2004)

20. Koh, K-H., Filippi, S., Griffin, J.H., Akay, A.: Characterization of turbine blade friction dampers. J. Eng. Gas Turbines Power **127**, 856–862 (2005)

21. Menq, C.H., Griffin, J.H.: A comparison of transient and steady state finite element analyses of the forced response of a frictionally damped beam. J. Vib. Acoust. Stress Reliab. Des. **107**, 19–25 (1985)

22. Tanrıkulu, Ö., Kuran, B., Özgüven, H.N., İmregün, M.: Forced harmonic response analysis of nonlinear structures using describing functions. AIAA J. **31**, 1313–1320 (1993)

23. Sanliturk, K.Y., Ewins, D.J., Elliott, R., Green, J.S.: Friction damper optimization: simulation of rainbow tests. J. Eng. Gas Turbines Power **123**, 930–939 (2001)

24. Ciğeroğlu, E., Özgüven, H.N.: Nonlinear vibration analysis of bladed disks with dry friction dampers. J. Sound Vib. **295**, 1028–1043 (2006)

25. Yang, M.T., Griffin, J.H.: A reduced order approach for the vibration of mistuned bladed disk assemblies. J. Eng. Gas Turbines Power **119**, 161–167 (1997)

26. Bladh, R., Castanier, M.P., Pierre, C.: Component-mode-based reduced order modeling techniques for mistuned bladed disks-part I: theoretical models. J. Eng. Gas Turbines Power **123**, 89–99 (2001)

27. Bladh, R., Castanier, M.P., Pierre, C.: Component-mode-based reduced order modeling techniques for mistuned bladed disks-part I: application. J. Eng. Gas Turbines Power **123**, 100–108 (2001)